Gabash, Aouss; Li, Pu:

On variable reverse power flow-part II: an electricity market model considering wind station size and location

Original published in:

Energies : open-access journal of related scientific research, technology development and studies in policy and management. - Basel : MDPI. - 9 (2016), 4, art. 235, 13 p.

ISSN: 1996-1073

DOI: 10.3390/en9040235

URL: http://dx.doi.org/10.3390/en9040235

[Visited: 2016-06-14]

energies

MDPI

Article

On Variable Reverse Power Flow-Part II: An Electricity Market Model Considering Wind Station Size and Location

Aouss Gabash * and Pu Li

Department of Simulation and Optimal Processes, Institute of Automation and Systems Engineering, Ilmenau University of Technology, Ilmenau 98693, Germany; pu.li@tu-ilmenau.de

* Correspondence: aouss.gabash@tu-ilmenau.de; Tel.: +49-3677-69-2813; Fax: +49-3677-69-1434

Academic Editor: Rodolfo Araneo

Received: 23 November 2015; Accepted: 18 March 2016; Published: 25 March 2016

Abstract: This is the second part of a companion paper on variable reverse power flow (VRPF) in active distribution networks (ADNs) with wind stations (WSs). Here, we propose an electricity market model considering agreements between the operator of a medium-voltage active distribution network (MV-ADN) and the operator of a high-voltage transmission network (HV-TN) under different scenarios. The proposed model takes, simultaneously, active and reactive energy prices into consideration. The results from applying this model on a real MV-ADN reveal many interesting facts. For instance, we demonstrate that the reactive power capability of WSs will be never utilized during days with zero wind power and varying limits on power factors (PFs). In contrast, more than 10% of the costs of active energy losses, 15% of the costs of reactive energy losses, and 100% of the costs of reactive energy imported from the HV-TN, respectively, can be reduced if WSs are operated as capacitor banks with no limits on PFs. It is also found that allocating WSs near possible exporting points at the HV-TN can significantly reduce wind power curtailments if the operator of the HV-TN accepts unlimited amount of reverse energy from the MV-ADN. Furthermore, the relationships between the size of WSs, VRPF and demand level are also uncovered based on active-reactive optimal power flow (A-R-OPF).

Keywords: active-reactive energy losses; variable reverse power flow (VRPF); varying power factors (PFs); wind station size-location

1. Introduction

The extended active-reactive optimal power flow (A-R-OPF) with reactive power of wind stations (WSs) in [1,2] is utilized in this paper to analyze an electricity market model using a real medium-voltage active distribution network (MV-ADN) connected to a high-voltage transmission network (HV-TN), as shown in Figure 1. Our particular focus will be on the impact of charging (paying) schemes for reactive energy which are applied, typically, by transmission system operators for users connected to a HV-TN in Europe [3]. The power flow direction of the *forward*/*reverse* active P_{S1} and reactive Q_{S1} power at a slack bus S_1 is shown in Figure 1. In general, an operating point represents the measured apparent power, e.g., at the secondary side of a transformer (TR). It is to note that an operating point can be in one of the four quadrants shown in Figure 1, but without violating the maximum TR capability [4–7].

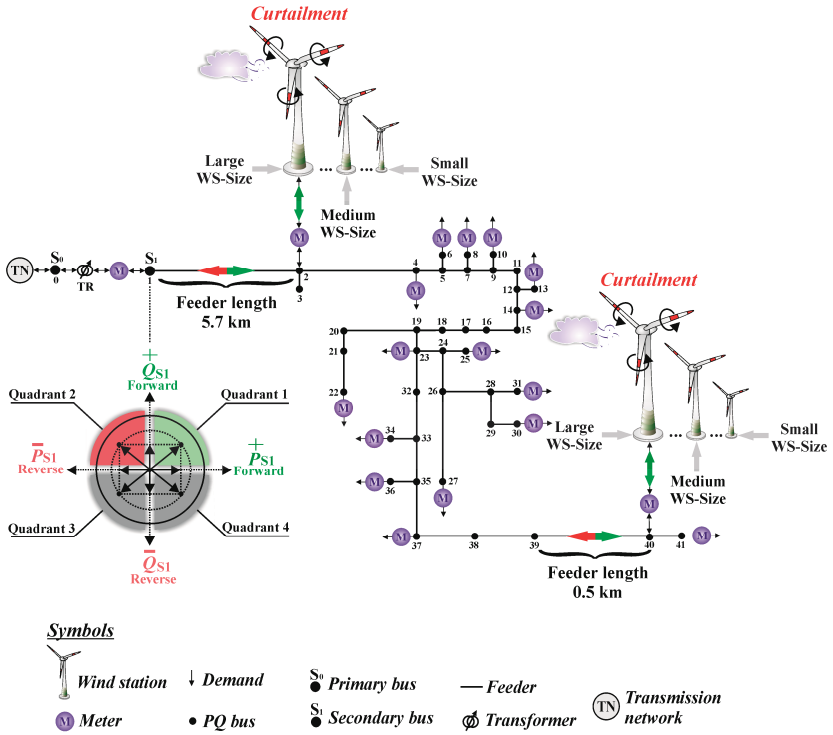

Figure 1. The medium-voltage active distribution network (MV-ADN) case study with active-reactive power flow direction definitions and capability diagram of a transformer (TR) at slack bus S_1 [5]. Here, different locations and sizes of a wind station (WS) are depicted to show the effect of variable reverse power flow (VRPF).

Recent studies [8–18] on reactive power planning and management, active power scheduling and losses, active distribution network (ADN) management, and *sizing* as well as *siting* distributed generation (DG) (e.g., WSs) show clearly the importance of variable reverse power flow (VRPF) in ADNs. However, it is also shown, e.g., in [12], that there are yet *no* definite answers on how exporting power to the upstream network or VRPF [1] can be accomplished. Therefore, the aim of this paper (Part-II), together with the companion paper (Part-I) [1], is to answer a few important questions related to this issue.

VRPF depends on many factors (e.g., the location and size of WSs, demand level, energy prices *etc.*), and therefore, to extract relationships between them by investigating these factors is not trivial. For this reason, we consider here a simplified WS model, as shown in Figure 2, inserted in the extended A-R-OPF model presented in Part-I [1].

The optimization problem to be solved in this paper contains a multi-objective function F (1) [1] with reactive power of WSs connected to the MV-ADN as shown in Figure 1:

$$\max_{\beta_{\text{c.w}}, Q_{\text{disp.w}}} \quad F = F_1 - F_2 - F_3 - F_4 - F_5 \tag{1}$$

$$F_1 = \sum_{h=1}^{T_{\text{final}}} C_{\text{pr.p}}(h) \sum_{\substack{i=1 \\ i \in I}}^{N} P_{\text{w}}(i,h)\beta_{\text{c.w}}(i,h) \tag{2}$$

$$F_2 = \sum_{h=1}^{T_{\text{final}}} C_{\text{pr.p}}(h)\, P_{\text{loss}}(h) \tag{3}$$

$$F_3 = \sum_{h=1}^{T_{\text{final}}} C_{\text{pr.q}}(h)\, Q_{\text{loss}}(h) \tag{4}$$

$$F_4 = \sum_{h=1}^{T_{\text{final}}} C_{\text{pr.p}}(h)\ P_{\text{S1}}(1,h) \tag{5}$$

$$F_5 = \sum_{h=1}^{T_{\text{final}}} C_{\text{pr.q}}(h)\ Q_{\text{S1}}(1,h) \tag{6}$$

Here, F_1 (2) is the total revenue from the injected wind active energy with P_{w} as the generated wind power of a wind turbine (WT), F_2 (3) is the total cost of active energy losses with P_{loss} as the active power losses in the MV-ADN, F_3 (4) is the total cost of reactive energy losses with Q_{loss} as the reactive power losses in the MV-ADN, F_4 (5) is the total cost/revenue of importing/exporting active energy at slack bus S_1 with P_{S1} as the active power produced/absorbed at slack bus S_1, and F_5 (6) is the total cost/revenue of importing/exporting reactive energy at slack bus S_1 with Q_{S1} as the reactive power produced/absorbed at slack bus S_1, as seen in Figure 1, respectively.

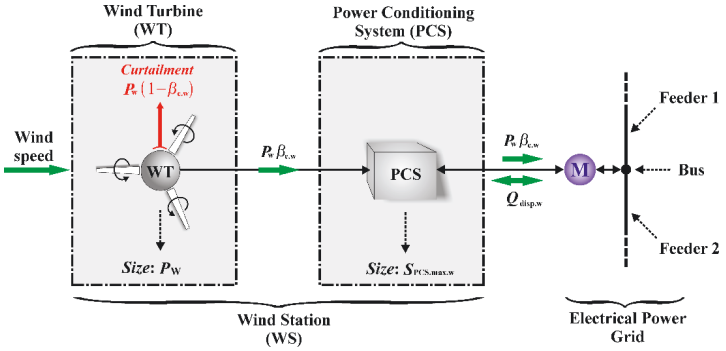

Figure 2. Simplified model of a WS [1]. Here, M stands for electrical meter and the wind turbine (WT) is connected to the grid through a full scale power converter or power conditioning system (PCS) as in [17] while the wind speed is converted to wind power P_{w} as in [5].

The above objective function is subject to *equality* and *inequality* constraints as given in Part-I [1]. Here, two control variables are considered. First, the curtailment factor $\beta_{\text{c.w}}$ ($0 \leqslant \beta_{\text{c.w}} \leqslant 1$) at a WS connected to the MV-ADN at a specific location or bus, see Figure 2. This factor is used for curtailing the wind active power generation to prevent violations of system constraints (detailed mathematical formulation is given in Part-I [1]). Second, the reactive power dispatch ($Q_{\text{disp.w}}$) of the WS, see Figure 2, which is to be optimized to minimize energy losses in the MV-ADN and meanwhile minimize the reactive energy import from the HV-TN [19,20]. More precisely, the curtailment factor and reactive power dispatch are used to balance all the terms in the objective function F (1) using an active energy price model $C_{\text{pr.p}}$ and a reactive energy price model $C_{\text{pr.q}}$ based on a meter-based A-R-OPF method [5]. The data of prices are given in Table A1 in the Appendix.

In this paper, we solve the optimization problem formulated above under the operating conditions defined in [1]. Particularly, we investigate the effect of varying upper bound of active power in reverse direction at slack bus S_1 denoted by $\alpha_{\text{P1.rev}}$ ($0 \leqslant \alpha_{\text{P1.rev}} \leqslant 1$), the lower power factors (PFs) of WSs denoted by $\text{PF}_{\text{min.w}}$ ($0 \leqslant \text{PF}_{\text{min.w}} \leqslant 1$) under different WS-sizes and WS-locations. Detailed data of the WS are given in Table A2 in the Appendix. After solving the problem different operating points can be obtained and their features distinguished:

- An operating point in the *green* quadrant 1 (see Figure 1) means that *both* active and reactive energies are being imported from the HV-TN to the MV-ADN.
- An operating point in the *red* quadrant 2 means that *only* active power is being exported from the MV-ADN to the HV-TN, while reactive energy is still imported [1].
- In this paper, we consider the situation that an operating point in the *gray* quadrants (*i.e.*, quadrants 3 and 4) should be avoided to minimize charging costs for reverse reactive energy [3].

However, if reverse reactive energy is being remunerated, as in the practice in some countries, a huge amount of reverse reactive energy could be observed as shown in [21].

2. Electricity Market Model

The electricity market model in this paper is defined as agreements between the MV-ADN (operator/company) and the HV-TN (operator/company) for *both* active and reactive energies [5]. It is to note here that the user of this method is the MV-ADN company/operator considering the operating and market conditions defined in Part-I [1]. Note that in an electricity market locational marginal prices (LMPs) can include many terms, e.g., system marginal energy cost, marginal cost of congestion and marginal cost of losses [5], and therefore, fixed active and reactive energy prices are used in this paper for clarity and simplicity.

2.1. Active Energy

The *forward* active energy from the HV-TN to the MV-ADN is to be minimized based on an active energy price model $C_{\mathrm{pr.p}}$, while the *reverse* active energy is either not allowed (*i.e.*, $\alpha_{\mathrm{P1.rev}} = 0$) in order to avoid any possible active power rejection as shown in [18], or allowed (*i.e.*, $0 < \alpha_{\mathrm{P1.rev}} \leqslant 1$) without any active power rejection as considered in [19,20].

2.2. Reactive Energy

The *forward* reactive energy is to be minimized based on a reactive energy price model $C_{\mathrm{pr.q}}$, while the *reverse* reactive energy (e.g., from WSs) is not allowed, in contrary to [21], in order to avoid any possible charge (payment) for capacitive reactive energy, e.g., as the case in Norway [3].

3. WS-Location in MV-ADN with Relation to Variable Reverse Power Flow

In order to uncover the relationship between the *WS-location* and *VRPF* under *feeder congestion*, the data of the power distribution network studied in [4,5] is extended here with *short-feeders* [1], as given in Table A3 in the Appendix. The feeders are represented by a single phase equivalent-π circuit. The peak power demand is assumed to be 16.25 MVA [4,5] with an upper bound of apparent power 20 MVA at slack bus S_1. The demand profiles are the same as described in Part-I [1].

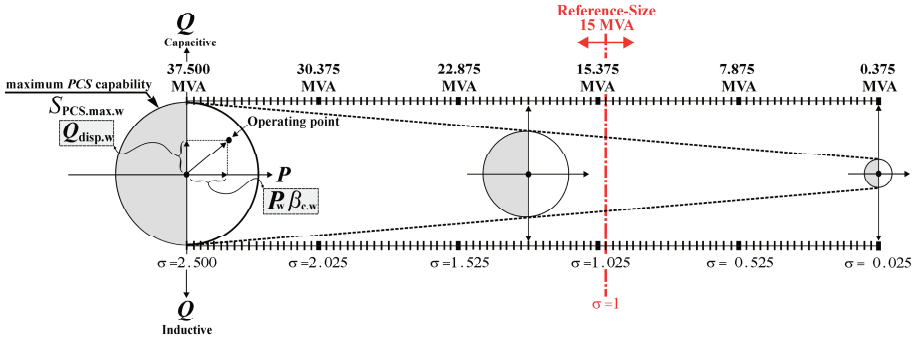

Figure 3. Illustration of 100 different sizes of a WS. Note that the size of a wind turbine (WT) is considered to be equal to the size of a PCS [1] and the WS-size is considered to be equal to a wind power plant (WPP) [17].

For clarity, we consider at first one WS consisting of one WT [22–24] with rated active power $P_{\mathrm{W}} = 15$ MW and one power conditioning system (PCS) unit with rated apparent power $S_{\mathrm{PCS.max.w}} = 15$ MVA. This WS-size is called in this paper *reference-size*, see Figure 3. The WS is connected to the network *either* at bus 2 *or* at bus 40, as shown in Figure 1. In this way, we can investigate the whole effect of VRPF. It is important to note that the voltage amplitude at slack bus S_1 has a significant impact on the grid power losses and on the feasibility of the optimization problem as shown in [5]. Therefore, we fix

this voltage amplitude in this paper at 1.02 pu and zero angle for all conducted computations. All other buses are considered as active power P and reactive power Q (PQ) buses, as shown in Figure 1.

4. WS-Size in MV-ADN with Relation to Variable Reverse Power Flow

To investigate the relationship between the maximum feasible *WS-size* and *VRPF* under *zero wind power curtailment*, we force the curtailment factor to be equal to 1 (*i.e.*, $\beta_{c.w} = 1$) in the extended A-R-OPF model. In other words, *no* wind power curtailment is allowed in the extended A-R-OPF model [1]. Note that wind power curtailment will happen *not only* at very low power demand *but also* in a strong relation with VRPF. Therefore, for the first time, we extract these relations by considering 100 different WS-sizes (see Figure 3) for the 2 different WS-locations (see Figure 1). This is achieved by carrying out the following steps:

(1) Choose a WS-location (e.g., bus 2) and provide a daily generated wind power profile (P_w) as input to the A-R-OPF model. This profile is selected from a day with relatively high wind speed to study the effect when the generated wind power equals to the rated power of the WT as seen in Figure 2.
(2) Assign a value to the allowed level of reverse active power flow, e.g., $\alpha_{P1.rev} = 0$, which is determined by an agreement.
(3) Start with the smallest WS-size (e.g., $P_W = 0.375$ MW and $S_{PCS.max.w} = 0.375$ MVA) and scale the wind power profile P_w provided in step 1 using σP_w, where σ is a *discrete* scaling factor corresponding to the WS-size, as depicted in Figure 3.
(4) If the A-R-OPF model is feasible (*i.e.*, an optimal solution is found for the selected WS-size and without the need to relax the control variable $\beta_{c.w}$ (*i.e.*, $0 \leqslant \beta_{c.w} \leqslant 1$), increase the WS-size and solve the corresponding problem.
(5) Repeat step 4 until a WS-size at which the model is infeasible (*i.e.*, the generated wind power should be curtailed, otherwise system constraints will be violated).
(6) The maximum WS-size found (*before* reaching infeasibility) is saved.

The above steps are repeated for two WS-locations (i.e., at bus 2 *or* 40) and different demand levels (from low to high) as shown in the case studies below. Another notice is that the available WS-sizes in the practice can be different from a manufacturer to another, see e.g., [22–24].

5. Case Studies

The analysis shown in this section is based on a *one-day* scenario with *hourly-discretization*. The optimization problem is solved by the general algebraic modeling system (GAMS) using the nonlinear programming (NLP) solver CONOPT3 as in [19,20]. The computation is carried out on a desktop with Intel 3.40 GHz (4-core) 16.00 GB RAM with circa 25 s for each program run. The results are transferred to and illustrated by using MATLAB [5]. The usual flat start (initialization) of variables is used in this work like in [19]. Different case studies due to different WS-locations are curried out and the results are given in Tables 1–8 and depicted in Figures 4–8 respectively.

Table 1. Objective function values for $\alpha_{P1.rev} = 0$, demand (100%) and wind power (100%) at bus 2. Active-Reactive optimal power flow: A-R-OPF.

Criterion	F_1 \$/day	F_2 \$/day	F_3 \$/day	F_4 \$/day	F_5 \$/day	F \$/day
A-R-OPF $PF_{min.w} = 1$	12,898	105	−6	5173	942	6647
A-R-OPF $PF_{min.w} = 0.85$	12,885	132	4	5158	158	7470
Difference	−13 (−**0.10%**)	+29 (**+21.80%**)	+10 (**+250%**)	+15 (**+0.28%**)	+784 (**+83.23%**)	+823 (**+12.40%**)

Table 2. Objective function values for $\alpha_{P1.rev}$ = 0.5, demand (100%) and wind power (100%) at bus 2.

Criterion	F_1 $/day	F_2 $/day	F_3 $/day	F_4 $/day	F_5 $/day	F $/day
A-R-OPF $PF_{min.w}$ = 1	14,910	141	7	3169	944	10,649
A-R-OPF $PF_{min.w}$ = 0.85	14,902	115	−3	3150	222	11,418
Difference	−8 (−**0.05%**)	+26 (**+18.44%**)	+10 (**+142.8%**)	+19 (**+0.60%**)	+722 (**+76.48%**)	+769 (**+7.22%**)

Table 3. Objective function values for $\alpha_{P1.rev}$ = 0.5, demand (100%) and wind power (**50%**) at bus 2.

Criterion	F_1 $/day	F_2 $/day	F_3 $/day	F_4 $/day	F_5 $/day	F $/day
A-R-OPF $PF_{min.w}$ = 0.85	7455	157	12	10,640	332	−3686
A-R-OPF $PF_{min.w}$ = 0	7455	150	9	10,633	**0.0**	−3337
Difference	0 (**0%**)	+7 (**+4.46%**)	+3 (**+25%**)	+7 (**+0.06%**)	+332 (**+100%**)	+349 (**+9.47%**)

Table 4. Objective function values for $\alpha_{P1.rev}$ = 0.5, demand (100%) and wind power (**0%**) at bus 2.

Criterion	F_1 $/day	F_2 $/day	F_3 $/day	F_4 $/day	F_5 $/day	F $/day
A-R-OPF $PF_{min.w}$ = 0.85	0	321	68	18,259	1006	-19,654
A-R-OPF $PF_{min.w}$ = 0	0	285	55	18,224	**0.0**	-18,564
Difference	0 (**0%**)	+36 (**+11.21%**)	+13 (**+19.12%**)	+35 (**+0.19%**)	+1006 (**+100%**)	+1090 (**+5.55%**)

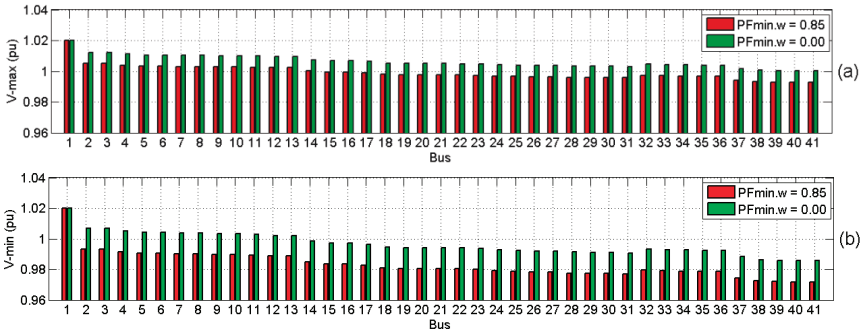

Figure 4. The maximum (**a**) and minimum (**b**) voltage amplitude of all buses corresponding to the case study in Table 4. Note 1: the voltage amplitude at slack bus S_1 is fixed at 1.02 pu. Note 2: the lower and upper bounds of voltage amplitudes are 0.94 and 1.06 pu, respectively.

5.1. WS-location at Bus 2

Case 1: In this case, the reverse active energy is not allowed, *i.e.*, $\alpha_{P1.rev}$ = 0. The results of the original A-R-OPF model ($PF_{min.w}$ = 1) and the new model ($PF_{min.w}$ = 0.85) are compared.

The nominal input wind power (100%) and demand (100%) profiles are shown in Figure 5a, whereas the results are given in Table 1 and Figure 5b–g (left column). It can be observed that a balance between active and reactive power dispatch of the WS is obtained, as shown in Figure 5b,c (left column). However, not all generated wind power can be injected into the MV network due to the condition that reverse active power is not allowed. This can be obviously seen from Figure 5d (left column) where the curtailment factor is less than 1 over many hours. The effects of utilizing the reactive power of the WS can also be clearly seen from Figure 5e,f (left column).

As expected, the impact on the active power import at slack bus S_1 is negligible in comparison to that of the reactive power. Due to introducing the price of reactive energy the optimization tends to minimize the reactive energy import as much as possible. This effect can be seen in Figure 5g (left column) where the PF is at the lower limit, *i.e.*, 0.85 almost over the operation period. However, the PF becomes higher during the hours 11–14 because of the high wind power generation. From Table 1, one can observe from the values of the objective function and its terms that the costs of active F_2 and reactive F_3 energy losses and the costs of reactive energy import F_5 are quite low in comparison to those from the original model. It is noted that the loss of the revenue from wind generation F_1 is small compared with the total revenues F.

Case 2: Here, we use the same input data as in case 1, but the reverse active energy is allowed with $\alpha_{P1.rev}$ = 0.5. The results are given in Table 2 and Figure 5b–g (right column). Once again, the positive impacts of the new model are still present. High revenues are obtained from wind power F_1 because of less wind power curtailments. This is clearly seen in Figure 5d (right column) where the curtailment factor is mostly near 1. Note that during the hours (e.g., 14–15) with high wind power generation, the reverse active power flow is high as shown in Figure 5e (right column). This leads to import reactive power as seen in Figure 5f (right column) at approximately unity PF, see Figure 5g (right column).

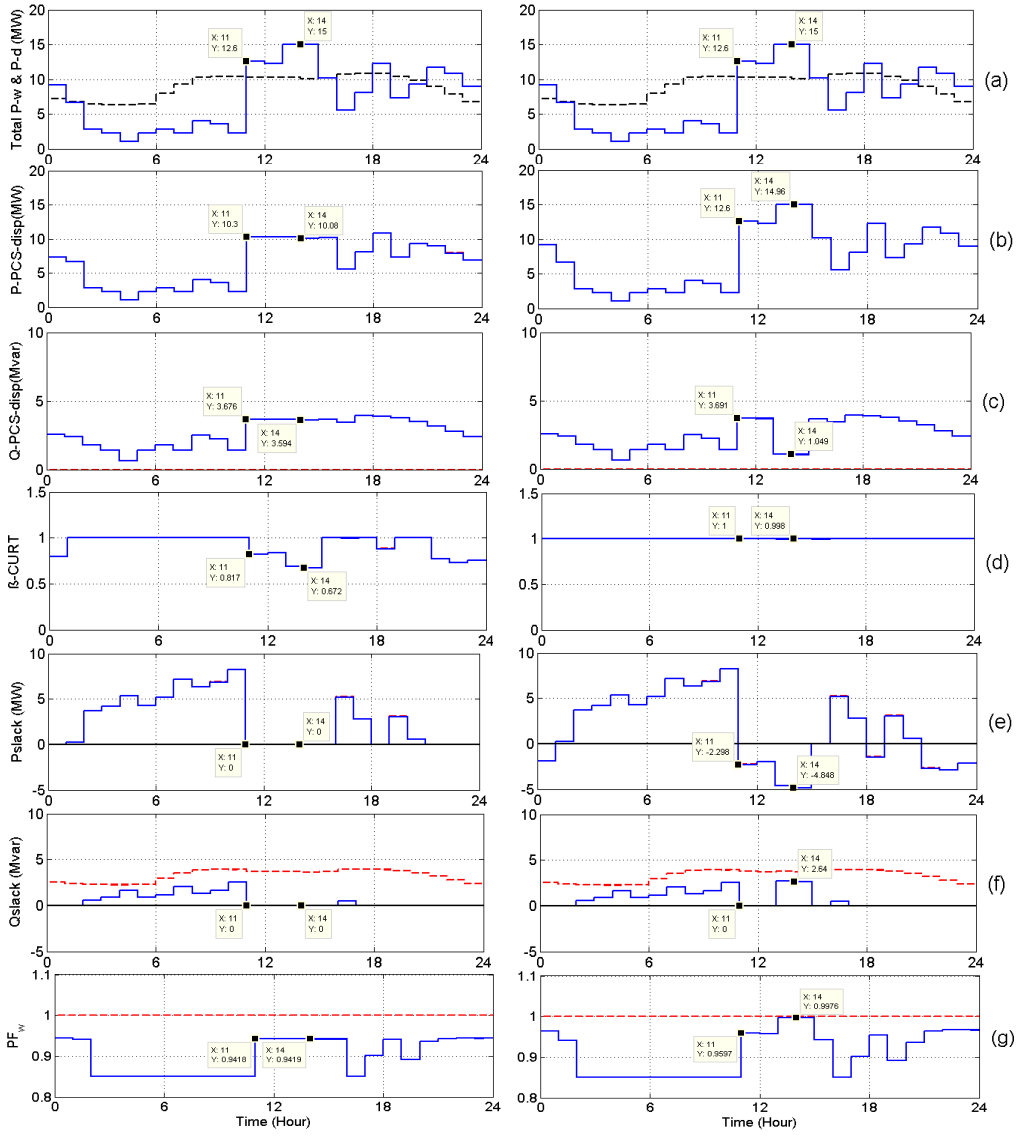

Figure 5. Trajectories by the extended and original A-R-OPF based on $\alpha_{P1.rev}$ = 0 (left column) and $\alpha_{P1.rev}$ = 0.5 (right column) at wind power (100%). (**a**) Wind power generation of the WS (solid-blue) and total demand power (dashed-black); (**b**) active power dispatch of the WS; (**c**) reactive power dispatch of the WS; (**d**) curtailment factor at the WS; (**e**) slack bus active power; (**f**) slack bus reactive power; (**g**) PF of the WS denoted by PF_w. Note: from (**b**) to (**g**) the lines (dashed-red) stand for the original A-R-OPF ($PF_{min.w}$ = 1) and (solid-blue) for the extended A-R-OPF ($PF_{min.w}$ = 0.85).

*Case*3: In this case, we use the same input data as in case 2, but the wind power generated is assumed to be lowered (50%) as seen in Figure 6a (left column). The results of the extended A-R-OPF model with ($PF_{min.w}$ = 0.85) and ($PF_{min.w}$ = 0) are compared, as given in Table 3 and Figure 6b–g (left column). It is aimed in this case to show the impacts of the new model if no limits are considered on

PFs. This effect is clearly seen in Figure 6c (left column) where the reactive power capability of the WS is fully utilized as a capacitor bank. Therefore, there is no need to import any reactive energy from the HV-TN, as seen in Figure 6f (left column). However, reactive energy needs to be imported if the available wind active power is too low to satisfy the lower bound $PF_{min.w} = 0.85$, as seen in Figure 6g (left column).

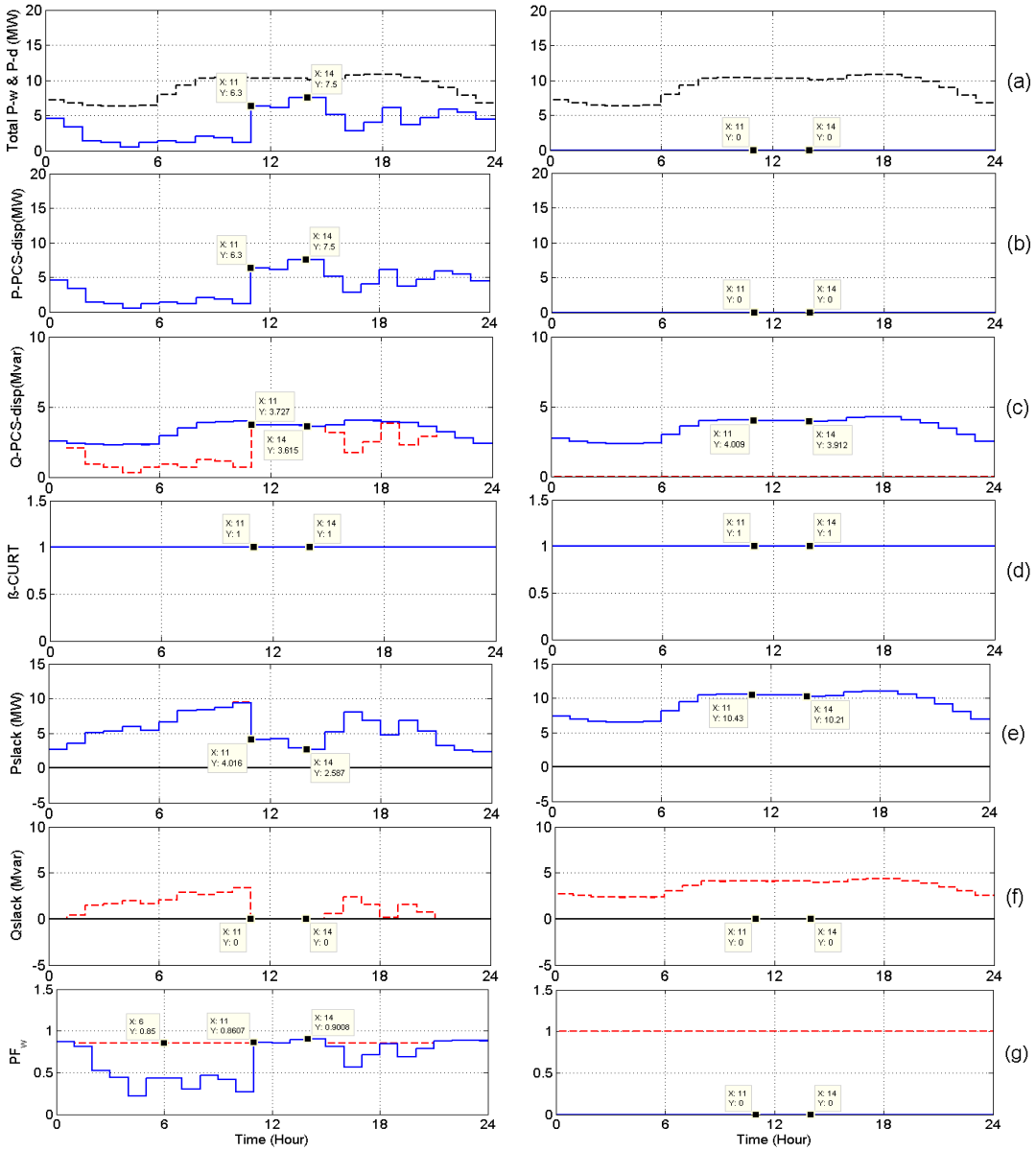

Figure 6. Trajectories by the extended A-R-OPF based on wind power (50%) (left column) and wind power (0%) (right column) at $\alpha_{P1.rev} = 0.5$. (**a**) Wind power generation of the WS (solid-blue) and total demand power (dashed-black); (**b**) active power dispatch of the WS; (**c**) Reactive power dispatch of the WS; (**d**) curtailment factor at the WS; (**e**) slack bus active power; (**f**) slack bus reactive power; (**g**) PF of the WS denoted by PF_w. Note: from (**b**) to (**g**) the lines (dashed-red) stand for the extended A-R-OPF ($PF_{min.w} = 0.85$) and (solid-blue) for the extended A-R-OPF ($PF_{min.w} = 0$).

The major benefit from this case is that it leads to a zero cost of reactive energy import F_5, as given in Table 3. Because of the low wind power generation in this case, no wind power curtailment occurs, as seen in Figure 6d (left column).

*Case*4: Here, the same input data as in case 3 are used, but the input wind power is set to zero (0%) as seen in Figure 6a (right column). It can be clearly seen that the reactive power capability of

the WS will be never utilized in this case if a limit on PF (e.g., $PF_{min.w} = 0.85$) is considered, as seen in Figure 6c (right column). This leads to a huge cost of reactive energy import F_5, as given in Table 4 in comparison to the case of $PF_{min.w} = 0$. In the latter case, the WS works as a capacitor bank to satisfy the needed reactive energy demand and also to minimize active F_2 and reactive F_3 energy losses, as given in Table 4. The maximum/minimum voltage amplitudes at all buses for this case study are illustrated in Figure 4. It is clearly seen that the extended model with $PF_{min.w} = 0$ makes the WS work as a capacitor bank to improve the voltage stability.

Case 5: In this case, we are interested in how the revenues/costs will change due to variable reverse active power flow at slack bus S_1 (*i.e.*, $F_4 + F_5$). Figure 7 (left-chart) shows clearly this effect. It can be seen that the costs (positive values), revenues (negative values), and the benefits of the extended A-R-OPF model highly depend on the demand level and the level of allowed reverse active power flow to the HV-TN. A *saturation* occurs depending on the demand level, e.g., at $\alpha_{P1.rev} = 0$ for high demand (150%). In contrast, the *saturation* occurs at $\alpha_{P1.rev} = 0.5$ and 0.7 for demand (50% and 10%), respectively.

5.2. WS-Location at Bus 40

The same 5 case studies for the WS-location at bus 2 are carried out for the WS-location at bus 40 and the results are shown in Figure 7 (right-chart) and given in Tables 5–8. Figure 7 shows clearly the effect of the location of the WS.

It can be seen that the costs, revenues and benefits of the extended A-R-OPF model highly depend on the demand level, WS-location, and the level of allowed reverse active power flow to the HV-TN. A *saturation* occurs depending on the demand level, e.g., at $\alpha_{P1.rev} = 0$ for high demand (150%) when the WS located at bus 2 *or* 40. In contrast, the *saturation* occurs at $\alpha_{P1.rev} = 0.3$ for both demand levels (50% and 10%) if no reactive power of WSs is considered. But if the reactive power of WSs is optimized, allowing a higher reverse active power flow leads to a higher cost reduction, especially at lower demand. One can also see and compare the differences between the results give in Tables 1–4 (for the WS-location at bus 2) and those in Tables 5–8 (for the WS-location at bus 40). The effect of *feeder congestion* is clearly seen from Tables 3 and 7 where the costs of reactive energy import F_5 is not totally (*i.e.*, 100%) avoided in the case of the WS-location at bus 40. This is because the WS is located far away from the exporting position S_1 in comparison to the WS located near S_1., *i.e.*, at bus 2.

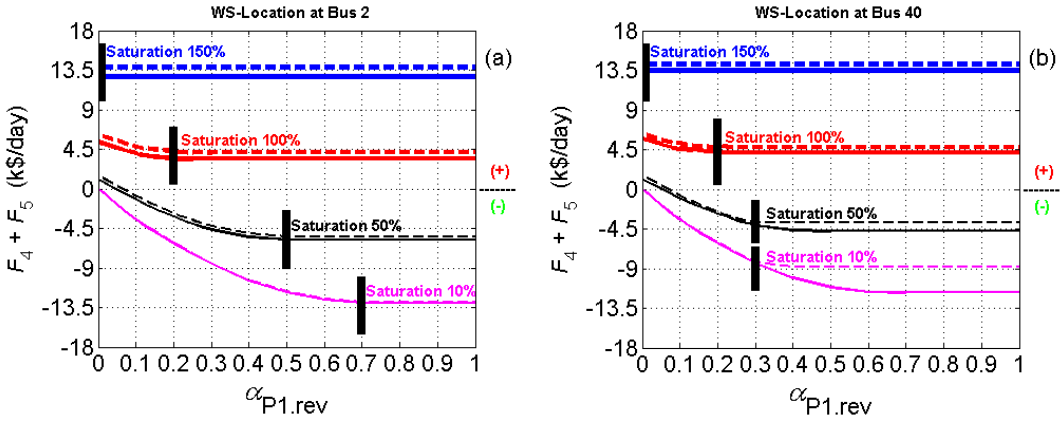

Figure 7. Relationships between $(F_4 + F_5)$ and $\alpha_{P1.rev}$ at wind power (100%) for the WS at bus 2 (**a**) or the WS at bus 40 (**b**). Note 1: the lines (dashed) stand for the original A-R-OPF ($PF_{min.w} = 1$) and (solid) for extended A-R-OPF ($PF_{min.w} = 0.85$). Note 2: for the demand level, lines (blue) stand for demand (150%), (red) for (100%), (black) for (50%) and (magenta) for (10%). Note 3: the *positive* values mean *costs* while *negative* values mean *revenues*.

Table 5. Objective function values for $\alpha_{P1.rev}$ = 0, demand (100%) and wind power (100%) at bus 40.

Criterion	F_1 $/day	F_2 $/day	F_3 $/day	F_4 $/day	F_5 $/day	F $/day
A-R-OPF $PF_{min.w}$ = 1	13,101	414	82	5251	1020	6334
A-R-OPF $PF_{min.w}$ = 0.85	13,082	384	71	5240	461	6926
Difference	−19 (−**0.15%**)	+30 (**+7.25%**)	+11 (**+13.41%**)	+11 (**+0.21%**)	+559 (**+54.8%**)	+592 (**+9.35%**)

Table 6. Objective function values for $\alpha_{P1.rev}$ = 0.5, demand (100%) and wind power (100%) at bus 40.

Criterion	F_1 $/day	F_2 $/day	F_3 $/day	F_4 $/day	F_5 $/day	F $/day
A-R-OPF $PF_{min.w}$ = 1	14,910	584	133	3612	1071	9510
A-R-OPF $PF_{min.w}$ = 0.85	14,909	556	123	3585	601	10,044
Difference	−1 (−**0.006%**)	+28 (**+4.8%**)	+10 (**+7.5%**)	+27 (**+0.75%**)	+470 (**+43.88%**)	+534 (**+5.62%**)

Table 7. Objective function values for $\alpha_{P1.rev}$ = 0.5, demand (100%) and wind power (50%) at bus 40.

Criterion	F_1 $/day	F_2 $/day	F_3 $/day	F_4 $/day	F_5 $/day	F $/day
A-R-OPF $PF_{min.w}$ = 0.85	7455	209	24	10,693	377	−3848
A-R-OPF $PF_{min.w}$ = 0	7455	244	33	10,727	50	−3599
Difference	0 (**0.0%**)	−35 (−**16.75%**)	−9 (−**37.5%**)	−34 (−**0.32%**)	+327 (**+86.74%**)	+249 (**+6.47%**)

Table 8. Objective function values for $\alpha_{P1.rev}$ = 0.5, demand (100%) and wind power (0%) at bus 40.

Criterion	F_1 $/day	F_2 $/day	F_3 $/day	F_4 $/day	F_5 $/day	F $/day
A-R-OPF $PF_{min.w}$ = 0.85	0	321	68	18,259	1006	−19,654
A-R-OPF $PF_{min.w}$ = 0	0	376	80	18,314	0.0	−18,770
Difference	0 (**0.0%**)	−55 (−**17.13%**)	−12 (−**17.65%**)	−55 (−**0.3%**)	+1006 (**+100%**)	+884 (**+4.5%**)

5.3. The Impact of WS-Size at Bus 2 or Bus 40

Here, we investigate the impact of the 100 WS-sizes defined in Figure 3 at two WS-locations, namely bus 2 *or* bus 4, to extract its relations to VRPF. It is aimed to find the maximum feasible WS-size (at a specific location) without violating system constraints. For this reason, the curtailment factor $\beta_{c.w}$ is set to 1 in this sub-section, *i.e.*, *no* wind power curtailment is allowed in all cases as explained above. The results are given in Table 9 and shown in Figure 8.

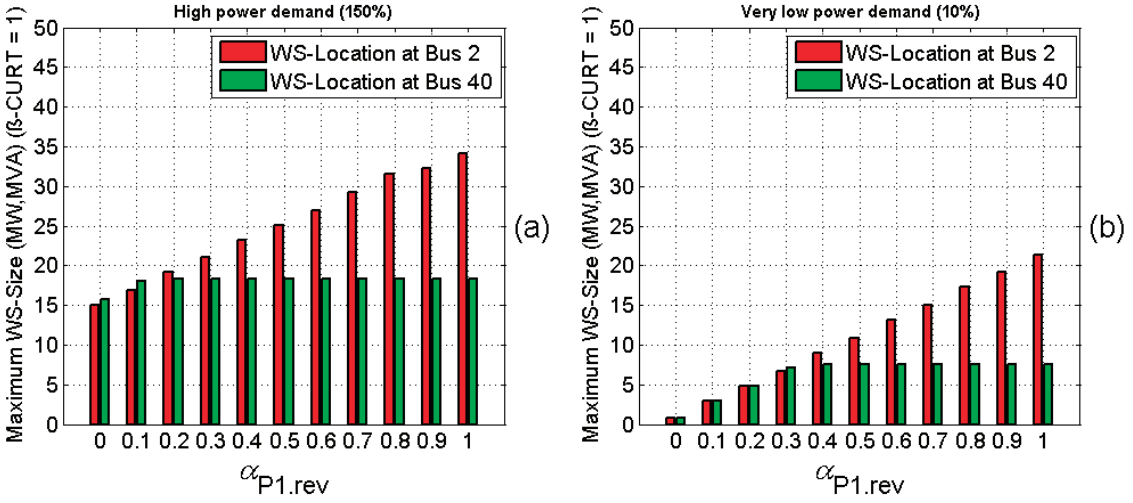

Figure 8. Ilustration of the reseuls in Table 9. Note that all scenarios are carried out at $PF_{min.w}$ = 0.85, $\beta_{c.w}$ = 1, high demand (150%) (**a**) and very low demand (10%) (**b**).

Table 9. The maximum feasible WS-Size (in MW for P_W and MVA for $S_{PCS.max.w}$) according to $\alpha_{P1.rev}$ at different WS-locations and demand levels.

$\alpha_{P1.rev}$	**0.0**	**0.1**	**0.2**	**0.3**	**0.4**	**0.5**	**0.6**	**0.7**	**0.8**	**0.9**	**1.0**
Bus 2 and 10% demand	0.750	3.0	4.875	6.75	9.0	10.875	13.125	15.0	17.250	19.125	21.375
Bus 40 and 10% demand	0.750	3.0	4.875	7.125	7.5	7.5	7.5	7.5	7.5	7.5	7.5
Bus 2 and 150% demand	15.0	16.875	19.125	21.0	23.25	25.125	27.0	29.250	31.50	32.250	34.125
Bus 40 and 150% demand	15.750	18.0	18.375	18.375	18.375	18.375	18.375	18.375	18.375	18.375	18.375

The results show clearly how *agreed/allowed* levels of reverse power flow affect the choice of the maximum feasible WS-size at a defined location. Another important fact is that the demand level in the MV-ADN also plays an important role. For example, if the demand connected to the MV-ADN is high, large WS-sizes will be feasible without any wind power curtailment. In addition, if the HV-TN operator/company agrees to accept the maximum level of reverse energy, *i.e.*, at $\alpha_{P1.rev} = 1$, the MV-ADN operator/company will install large WS-sizes. In summary, planning and operating a MV-ADN with high penetration of wind power requires a well-defined agreement for *forward/reverse active/reactive* power flow *from/to* the HV-TN.

6. Conclusions

In this paper, we have presented the relationships and the interplay between wind generation curtailment, VRPF, varying PFs of WSs, different demand levels, and active/reactive energy prices in an electricity market model under different scenarios. It is shown that the extended A-R-OPF allows WSs to provide reactive power as, e.g., capacitor banks and battery storage systems. In addition, we derived based on computation results clear rules for power system planners when VRPF is allowed. Moreover, it is shown that reactive reverse power flow will be minimized by using the developed model to avoid any possible charge for reverse reactive energy. Moreover, the reactive power of WSs can be utilized for avoiding extra costs of investments for reactive power provision. Furthermore, optimizing the reactive power flow according to the location of WSs can reduce huge costs, especially in the case of low demand, high wind power generation, and a high level of allowed reverse active power flow. This can be achieved with a well-defined *reverse active power flow agreement* between different power system operators in electricity markets. Finally, strong relationships between WS-sizes/WS-locations, VRPF and demand level are shown. As a result, the level of allowed reverse power flow will strongly affect the final decision when planning a high penetration of wind power.

Acknowledgments: We acknowledge support for the Article Processing Charge by the German Research Foundation and the Open Access Publication Fund of the Technische Universität Ilmenau.

Author Contributions: The corresponding author (A. Gabash) developed the model, wrote the code and performed the computation; both authors (A. Gabash and P. Li) wrote the paper.

Conflicts of Interest: The authors declare no conflict of interest.

Appendix

Table A1. Data of energy prices [5].

Period	$C_{pr.p}$ **($/MWh)**	$C_{pr.q}$ **($/Mvarh)**
From 12:00 (a.m.) to 07:00 (a.m.)	50	12
From 07:00 (a.m.) to 09:00 (p.m.)	100	12
From 09:00 (p.m.) to 12:00 (a.m.)	50	12

Table A2. Data of WT, PCS capability and limits on power factors (PFs) for WS.

P_W	$S_{PCS.max.w}$
0.375–37.500 MW(100 sizes)	0.375–37.500 MVA(100 sizes)
$PF_{min.w}$	$PF_{max.w}$
(0, 0.85, 1) lag/lead	1

Table A3. Extended data of the real 41-bus/40-feeder/27.6 kV network, see [1,4,5].

No. line	From bus	To bus	Line type	Length (km)	R_l (ohm/km)	X_l (ohm/km)	B_l (μs/km)	Ampacity (MVA)
1	**1**	**2**	**L1**	5.7000	0.169111	0.418206	3.9540	**20**
2	**2**	**3**	**L1**	1.0100	0.169111	0.418206	3.9540	**20**
3	**2**	**4**	**L1**	0.4000	0.169111	0.418206	3.9540	**20**
4	**4**	**5**	**L1**	0.3800	0.169111	0.418206	3.9540	**20**
5	**5**	**6**	**L1**	0.1300	0.169111	0.418206	3.9540	**20**
6	**5**	**7**	**L1**	0.1700	0.169111	0.418206	3.9540	**20**
7	**7**	**8**	**L1**	0.0010	0.169111	0.418206	3.9540	**20**
8	**7**	**9**	**L1**	0.2600	0.169111	0.418206	3.9540	**20**
9	**9**	**10**	**L1**	0.1400	0.169111	0.418206	3.9540	**20**
10	**9**	**11**	**L1**	0.3800	0.169111	0.418206	3.9540	**20**
11	**11**	**12**	**L1**	0.5600	0.169111	0.418206	3.9540	**20**
12	**12**	**13**	**L1**	0.3000	0.169111	0.418206	3.9540	**20**
13	**12**	**14**	**L1**	3.3300	0.169111	0.418206	3.9540	**20**
14	**14**	**15**	**L1**	1.0300	0.169111	0.418206	3.9540	**20**
15	**15**	**16**	**L1**	0.0010	0.169111	0.418206	3.9540	**20**
16	**16**	**17**	**L1**	1.0800	0.169111	0.418206	3.9540	**20**
17	**17**	**18**	**L1**	1.6400	0.169111	0.418206	3.9540	**20**
18	**18**	**19**	**L1**	0.4700	0.169111	0.418206	3.9540	**20**
19	**19**	**20**	**L3**	0.4700	0.348124	0.468482	3.7571	**14.3**
20	**20**	**21**	**L3**	0.0010	0.348124	0.468482	3.7571	**14.3**
21	**21**	**22**	**L5**	0.9600	1.391924	0.478811	3.5971	**1**
22	**19**	**23**	**L3**	0.1900	0.348124	0.468482	3.7571	**14.3**
23	**23**	**24**	**L3**	1.9400	0.348124	0.468482	3.7571	**14.3**
24	**24**	**25**	**L3**	2.4500	0.348124	0.468482	3.7571	**14.3**
25	**24**	**26**	**L3**	1.6300	0.348124	0.468482	3.7571	**14.3**
26	**26**	**27**	**L4**	1.2000	0.552276	0.485241	3.6035	**2**
27	**26**	**28**	**L3**	2.1200	0.348124	0.468482	3.7571	**14.3**
28	**28**	**29**	**L4**	0.7300	0.552276	0.485241	3.6035	**2**
29	**29**	**30**	**L4**	0.7500	0.552276	0.485241	3.6035	**2**
30	**28**	**31**	**L3**	2.5400	0.348124	0.468482	3.7571	**14.3**
31	**23**	**32**	**L2**	0.3600	0.276519	0.458580	3.8280	**16**
32	**32**	**33**	**L2**	0.2600	0.276519	0.458580	3.8280	**16**
33	**33**	**34**	**L4**	3.5800	0.552276	0.485241	3.6035	**2**
34	**33**	**35**	**L2**	0.7700	0.276519	0.458580	3.8280	**16**
35	**35**	**36**	**L3**	2.0800	0.348124	0.468482	3.7571	**14.3**
36	**35**	**37**	**L2**	4.5100	0.276519	0.458580	3.8280	**16**
37	**37**	**38**	**L1**	3.2400	0.169111	0.418206	3.9540	**20**
38	**38**	**39**	**L1**	0.3000	0.169111	0.418206	3.9540	**20**
39	**39**	**40**	**L1**	0.5000	0.169111	0.418206	3.9540	**20**
40	**40**	**41**	**L1**	0.0010	0.169111	0.418206	3.9540	**20**

References

1. Gabash, A.; Li, P. On variable reverse power flow-part I: Active-Reactive optimal power flow with reactive power of wind stations. *Energies* **2016**, *9*. [CrossRef]
2. Gabash, A.; Li, P. Variable reverse power flow-part II: Electricity market model and results. In Proceedings of the 2015 IEEE 15th International Conference on Environment and Electrical Engineering (EEEIC), Rome, Italy, 10–13 June 2015; pp. 27–32.

3. ENTSO-E Overview of transmission tariffs in Europe: Synthesis 2015. Available online: https://www.entsoe.eu (accessed on 26 February 2016).
4. Atwa, Y.M. Distribution System Planning and Reliability Assessment under High DG Penetration. Ph.D. Thesis, University of Waterloo, Waterloo, ON, Canada, 2010.
5. Gabash, A. *Flexible Optimal Operations of Energy Supply Networks: With Renewable Energy Generation and Battery Storage*; Südwestdeutscher Verlag: Saarbrücken, Germany, 2014.
6. Jayawardena, A.V.; Meegahapola, L.G.; Robinson, D.A.; Perera, S. Microgrid capability diagram: A tool for optimal grid-tied operation. *Renew. Energy* **2015**, *74*, 497–504. [CrossRef]
7. Arefifar, S.A.; Mohamed, Y.A.-R.I. DG mix, reactive sources and energy storage units for optimizing microgrid reliability and supply security. *IEEE Trans. Smart Grid* **2014**, *5*, 1835–1844. [CrossRef]
8. Singh, A.K.; Parida, S.K. Novel sensitivity factors for DG placement based on loss reduction and voltage improvement. *Electr. Power Energy Syst.* **2016**, *74*, 453–456. [CrossRef]
9. Sultana, S.; Roy, P.K. Krill herd algorithm for optimal location of distributed generator in radial distribution system. *Appl. Soft Comput.* **2016**, *40*, 391–404. [CrossRef]
10. Jordehi, A.R. Allocation of distributed generation units in electric power systems: A review. *Renew. Sustain. Energy Rev.* **2016**, *56*, 893–905. [CrossRef]
11. Prakash, P.; Khatod, D.K. Optimal sizing and siting techniques for distributed generation in distribution systems: A review. *Renew. Sustain. Energy Rev.* **2016**, *57*, 111–130. [CrossRef]
12. Stadler, M.; Cardoso, G.; Mashayekh, S.; Forget, T.; DeForest, N.; Agarwal, A.; Schönbein, A. Value streams in microgrids: A literature review. *Appl. Energy* **2016**, *162*, 980–989. [CrossRef]
13. Soroudi, A.; Siano, P.; Keane, A. Optimal DR and ESS scheduling for distribution losses payments minimization under electricity price uncertainty. *IEEE Trans. Smart Grid* **2016**, *7*, 261–272. [CrossRef]
14. Sedghi, M.; Ahmadian, A.; Aliakbar-Golkar, M. Optimal storage planning in active distribution network considering uncertainty of wind power distributed generation. *IEEE Trans. Power Syst.* **2016**, *31*, 304–316. [CrossRef]
15. Kim, S.W.; Kim, J.; Jin, Y.G.; Yoon, Y.T. Optimal bidding strategy for renewable microgrid with active network management. *Energies* **2016**, *9*. [CrossRef]
16. Garces, A. A quadratic approximation for the optimal power flow in power distribution systems. *Electr. Power Syst. Res.* **2016**, *130*, 222–229. [CrossRef]
17. IEC 61400–27–1. *Wind turbines – Part 27–1: Electrical simulation models –Wind turbines. Edition 1.0, 2015–02*; International Electrotechnical Commission: Geneva, Switzerland, 2015.
18. Gabash, A.; Xie, D.; Li, P. Analysis of influence factors on rejected active power from active distribution networks. In Proceedings of the IEEE Power & Energy Student Summit, Ilmenau, Germany, 19–20 January 2012; pp. 25–29.
19. Gabash, A.; Li, P. Active-Reactive optimal power flow in distribution networks with embedded generation and battery storage. *IEEE Trans. Power Syst.* **2012**, *27*, 2026–2035. [CrossRef]
20. Gabash, A.; Li, P. Flexible optimal operation of battery storage systems for energy supply networks. *IEEE Trans. Power Syst.* **2013**, *28*, 2788–2797. [CrossRef]
21. Gabash, A.; Li, P. Reverse active-reactive optimal power flow in ADNs: Technical and economical aspects. In Proceedings of the 2014 IEEE International Energy Conference (ENERGYCON), Cavtat, Croatia, 13–16 May 2014; pp. 1115–1120.
22. ENERCON Products. Available online: http://www.enercon.de (accessed on 26 February 2016).
23. Vestas Products. Available online: https://www.vestas.com (accessed on 26 February 2016).
24. SIEMENS Wind Power Platforms. Available online: http://www.energy.siemens.com (accessed on 26 February 2016).